CHEMICAL ENGINEERING TRANSACTIONS
VOL. 99, 2023
A publication of AIDIC
The Italian Association of Chemical Engineering
Online at www.cetjournal.it
Guest Editors: Sauro Pierucci, Flavio Manenti

ISBN 978-88-95608-98-3; **ISSN** 2283-9216
DOI: 10.3303/CET2399114

Characterization by XRD and FTIR of Zeolite A and Zeolite X Obtained from Fly Ash

Nelson W. Farro[a*], Wilson Reyes[a], Jorge L. Mendoza[a], Lucien Veleva[b], Patricia Quintana[b], José A. Azamar[b], Daniel Aguilar[b]

[a] Dept.of Chemistry, Faculty of Chemical Engineering, National University of Trujillo. Av. Juan Pablo II s/n. Trujillo, Perú
[b] Applied Physics Department, Center for Research and Advanced Studies (CINVESTAV), Mérida 97310, México
nfarro@unitru.edu.pe

Fly ashes from the fluidized bed boiler were used to obtain zeolites by the alkaline fusion process, followed by a hydrothermal procedure. The melting was carried out with 98 % granulated NaOH, mixed with ashes in mass ratios 1.2/1, 1.4/1 and 1.6/1 and using three melting temperatures, 450 °C, 550 °C and 650 °C. For the crystallization of the zeolites, the hydrothermal procedure at 90 °C was used. The crystalline phases of the zeolitic materials were quantified by XRD analysis. The morphology of the crystals was identified by SEM. The FTIR spectra revealed that the transformation of sodalite mineral to zeolite A and zeolite X increased with the NaOH/CVT ratio and the temperature.

1.Introduction

Fluidized bed boilers generate fly ash (FA), with a high percentage of unburned because of the operation process at almost ~850 °C, which does not allow the complete calcination of the coal (Janowska and Kaliciak, 2021). The high content of unburned material makes the ashes unfriendly to the environment, however, their transformation into zeolites is a very useful procedure. The hydrated zeolites exhibit a regular three-dimensional crystalline aluminosilicates structures based on tetrahedrons, where silicon or aluminum cation are surrounded by four oxygen atoms at the vertices, representing $[SiO4]^{4-}$ and $[AlO4]^{5-}$ (Byrappa and Yoshimura, 2013). These structures form a network of pores and channels, which make any zeolite a highly microporous material, adsorbing water and cations, depending on the diameter of the pores. Due to this property, zeolites have a wide application in separation and filtration industrial processes (Chaves et al., 2019). Zeolites may be obtained from fly ash, among others, by alkaline fusion, mixing them with solid NaOH or KOH, in mass ratios NaOH/FA = 1/1 to 2/1. Melted between 500 °C to 650 °C, and their posterior a hydrothermal stage between 60 °C and 150 °C helped the crystallization process, able to achieve different proportions of zeolites A and zeolites X (Shi and Chang, 2021). The identification and characterization of zeolites A and X have been done through their crystallinity percentages, by means of X-ray diffraction (XRD), scanning electron microscopy (SEM) and infrared spectroscopy (FTIR) (Akbelen, 2021). The magic-angle spinning magnetic resonance (MAS-NMR) spectra suggested that the sodalite configures the formation of quadrangular and hexagonal rings of D4R and D6R, respectively, which then will build the frameworks (Shigemoto, et al., 1995). In the present research, the zeolite A and zeolite X (XRD) were achieved by alkaline fusion of fly ash at three temperatures and three NaOH/FA ratios. Their crystallinity (XRD) and morphology (SEM) were quantified, followed by the IR spectra analysis, suggesting that structural changes occurred during the transformation of sodalite phase.

2. Material and methods

Fly ash from the fluidized bed boiler of the Trupal Cardboard Company (La Libertad, Peru) was used, which chemical composition is shown in Table 1.The samples, previously sieved at No. 80 ASTM mesh, were calcined for 3 h, at 600 °C, to eliminate the high percentage of unburned material. Part of the ashes was acid-washed with 3.5 M HCl (FATH samples), in order to promote dealumination and improve zeolitization (Hartati, et al., 2020). Both ashes, the acid-washed (FATH), and those without acid (FAT), were washed with distilled water,

Paper Received: 31 January 2023; Revised: 3 March 2023; Accepted: 6 May 2023
Please cite this article as: Farro N.W., Reyes W., Mendoza J.L., Veleva L., Quintana P., Azamar J.A., Aguilar D., 2023, Characterization by XRD and FTIR of Zeolite A and Zeolite X Obtained from Fly Ash, Chemical Engineering Transactions, 99, 679-684 DOI:10.3303/CET2399114

and the solid parts were separated by filtration. The FATH and FAT ashes were dried at 100 °C and after cooling they were coded for identification.

Table 1. Chemical composition of ash batch 10375 (YURA Cement Laboratory, Arequipa).

Component	SiO_2	Al_2O_3	K_2O	Fe_2O_3	TiO_2	Other oxides	LOI	Amorphous phases
%	44.50	27.38	1.87	1.63	1.44	2.35	20.82	42.7

2.1. Synthesis of zeolites

The alkaline fusion method was used, followed by a hydrothermal process. Mixtures of 98 % NaOH and FAT ashes, in NaOH/FAT mass ratios = 1.2/1.0; 1.4/1.0 and 1.6/1.0, were placed in three nickel crucibles. They were subjected to fusion, in a muffle, at a constant temperature of 450 °C, for 1 h. The procedure was repeated with other samples at 550 °C and 650 °C. For the samples of acid-ashes (FATH), the ratio NaOH/FATH = 1.6 was used, at a melting temperature of 550 °C. The fusion product was cooled, ground, and washed to remove residual NaOH. Then, the mixtures are brought to crystallization at 90 °C, leaving them to rest for 6 hours. The obtained zeolitic material (ZM) was filtered, washed, and neutralized with 1% HCl. The solids were separated by filtration and dried in an oven at 105 °C. They were cooled and placed in hermetic bags for analysis.

2.2. Characterization and identification of zeolites

For X-ray diffraction analysis, Bruker D8-Advance Diffractometer with 1 s step time, 2θ of 0.02 degrees, at 40 kV, 30 mA, CuKα radiation (λ = 1.5418 Å) was used. For crystal morphology, a scanning microscope (SEM) coupled with energy dispersive spectroscope for an elemental analysis by (EDS), JEOL JMS-7600F, was used. For the IR spectra, Thermo Nexus 670-FTIR Spectrometer was used, with near, medium and far infrared, with KBr pellet method.

3. Results and discussion

The XRD analysis of the zeolitic materials ZMs identified and quantified the crystalline phases, based on the relative intensities of the characteristic peaks of the spectra (Tables 2, 3 and 4).

Table 2. Composition of zeolitic materials ZMs, obtained at 450 °C, according to the XRD spectra

Ratio NaOH/FAT	Sodalite (%) (Na, CO_3, H_2O)	Hydroxy-sodalite (%)	Zeolite X (%)	Zeolite A (%)	Code ZM
1.2/1	51.2	37.2	11.7		ZM – 01
1.4/1	65.9		26.9	7.2	ZM – 02
1.6/1	24.0		39.9	36.1	ZM - 03

Table 3. Composition of zeolitic materials ZMs, obtained at 550 °C, according to XRD spectra

Ratio NaOH/FAT	Sodalite (%) (Na, CO_3, H_2O)	Thaumasite (%)	Zeolite-X (%)	Zeolite-A (%)	Code ZM
1.2/1	40.2	12.6	34.1	13.1	ZM – 04
1.4/1	59.5		29.8	10.7	ZM – 05
1.6/1	51.0		22.9	26.2	ZM – 06
(FATH) 6/1		-	7.0	93.0	ZM – 07*

Table 4. Composition of zeolitic materials ZMs, obtained at 550 °C, according to XRD spectra

Ratio NaOH/FAT	Sodalite (%) (Na, CO_3, H_2O)	Hydroxy-sodalite (%)	Zeolite-X (%)	Zeolite- A (%)	Code ZM
1.2/1			34.6	65.4	ZM – 08
1.4/1			34.3	65.7	ZM - 09
1.6/1			17.8	82.2	ZM - 10

3.1 Effect of NaOH/FAT ratio and temperature on the composition of the zeolitic materials

The main identified phases (Tables 2, 3 and 4) were sodalite, hydroxy-sodalite, zeolite X and zeolite A, which appeared at all melting temperatures, except the thaumasite phase only at 550 °C and at the lowest NaOH/FAT mass ratio = 1.2/1. The majority amount corresponds to both sodalite phases, at lower temperature and lower NaOH/FAT ratio. At 650 °C, the sodalite phases disappeared, leaving only zeolite A and zeolite X, which were

formed at any NaOH/FAT ratio, at all three temperatures. According to Table 2, at 450 °C the formation rate of zeolite X is much higher than that of A. However, this relationship is inverted as the melting temperature and the NaOH/FAT ratio increased: at 650 °C and NaOH/FAT = 1.6/1 the majority phase was zeolite A (82 %). The high thermal stability of zeolite A (Ma and Liu, 2022) is an important factor, according to which zeolite A forms in greater quantities after reaching 650 °C. At 90 °C, zeolite A crystallization is favored, but not that of zeolite X, which is a metastable and its crystallization is favored between 35 °C - 40 °C (Belviso, et al., 2010). On the other hand, Table 3 indicates that ZM-07, obtained from FATH, crystallized in 93 % of zeolite A, and without the existence of sodalite. These results agree with the research of Duan et al. (2011), suggesting that the high SiO_2/Al_2O_3 ratios may be obtained by a pretreatment of aluminosilicates with HCl acid, improving the crystallization of zeolites, by the removal of OH^-, Al^{3+} ions and iron impurities.

3.2. Zeolite morphology: scanning electron microscopy (SEM)

Figures 1 and 2 belong to SEM micrographs of ZM-03 and ZM-05, obtained at two different temperatures, but of equal NaOH/FAT ratio. The ZMs present cubic and octahedral crystals, surrounded by coalescing spheroidal grains, typical of sodalite phase (Pengcheng Lv, et al., 2021). Comparing the formation conditions of ZM-03 and ZM-05, the increased melting temperature from 450 °C to 550 °C favored the formation of zeolite A and zeolite *X*, at the expense of the decreased sodalite phase.

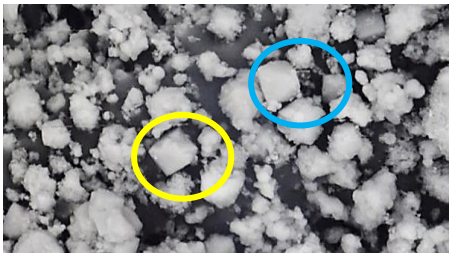

Figure 1. SEM micrograph (x2000) of ZM-03.

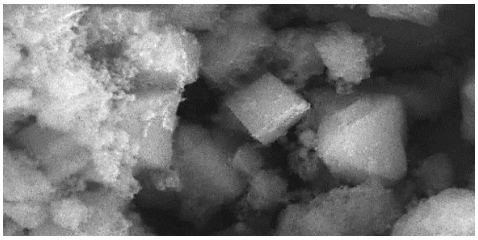

Figure 2. SEM micrograph (x7500) of ZM-05.

3.3. FTIR analysis of zeolitic materials

3.3.1. Zeolites ZM-01, ZM-02 and ZM-03

Figure 3 shows the IR spectra of the materials ZM-01, ZM-02 and ZM-03, produced according to the conditions given in Table 2. Since hydroxy-sodalite and sodalite have very similar crystalline structures (Hermeler, et al., 1991), the frequencies of the IR spectra are considered the same for both zeolites. According to Table 2, sodalite is present in all three zeolitic mixtures, which intense asymmetric stretching band at 989 cm^{-1} is typical of sodalite (Table 5). Likewise, the middle band of 699 cm^{-1} and the T-O bending band of 461 cm^{-1} of sodalite, are present in all three IR spectra (Figure 3). On the other hand, the zeolite X is detected with the symmetrical stretches corresponding to frequencies of 753 cm^{-1} and 699 cm^{-1} and especially with that of 565 cm^{-1}, which corresponds to the vibration of the double ring D6R of faujasite high silica zeolite (Zhan, et al., 2002) and it was detected in the spectra of the three samples (Figure 3). In the spectrum of ZM-02 at the frequency of 553 cm^{-1} was observed the double ring of D4R of zeolite (Loiola, et al., 2012). This frequency disappeared in the spectra of ZM-03, where the broad asymmetric stretching bands at 992 cm^{-1} and at 1051 cm^{-1} indicated the presence of zeolite A, as well as that at 464 cm^{-1}, characteristic for the T-O bending in ZM-03 zeolite. It has been reported that the at ~870cm^{-1} the shoulder band, which appears in the spectra of the three mixtures, is attributed to the vibration of T–OH bonds of the amorphous precursor, during the formation of zeolite A and zeolite X (Shigemoto, et al.,1995). The frequencies of the bands presented in Figure 3 confirmed the results of Table 2, which suggested that the presence of sodalite decreases, because it is transformed into zeolite A, as the NaOH/FAT ratio raises.

Table 5. IR spectra data for some synthetic zeolites (Flanigen and Khatami, 1974)

Sample	Asymmetric stretching **(*)** →Si–O–T→			Symmetric stretching ←Si–O–T→			Double ring	Bending T – O
Zeolite-A	1090*vwsh*	1050*vwsh*	995*s*			660*vw*	550*ms*	464*m*
Zeolite-X		1060*msh*	971*s*	746*m*	690*wsh*	668*m*	560*m*	458*ms*
Hydroxy sodalite	1096*vwsh*		986*s*	729*m*	701*mw*	660*m*		461*ms*

(*) T: Si or Al. *s: strong; m: medium; ms: medium-strong; w: weak; mw: medium-weak; vw: very weak; sh: shoulder:*

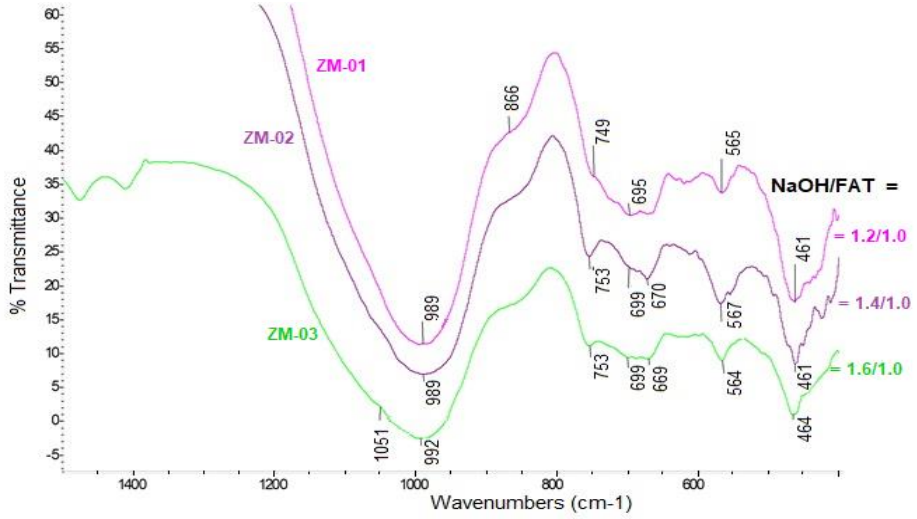

Figure 3. IR spectra of ZM-01, ZM-02 and ZM-03, obtained at 450ºC and at three increasing NaOH/FAT ratios.

3.3.2 Zeolites MZ-04, MZ-05 and MZ-06

Figure 4 presents the IR spectra of the zeolite samples ZM-04, ZM-05 and ZM-06, obtained at 550 ºC, with an increasing NaOH/FAT mass ratios = 1.2/1.0, 1.4/1.0 and 1.6/1.0, respectively.

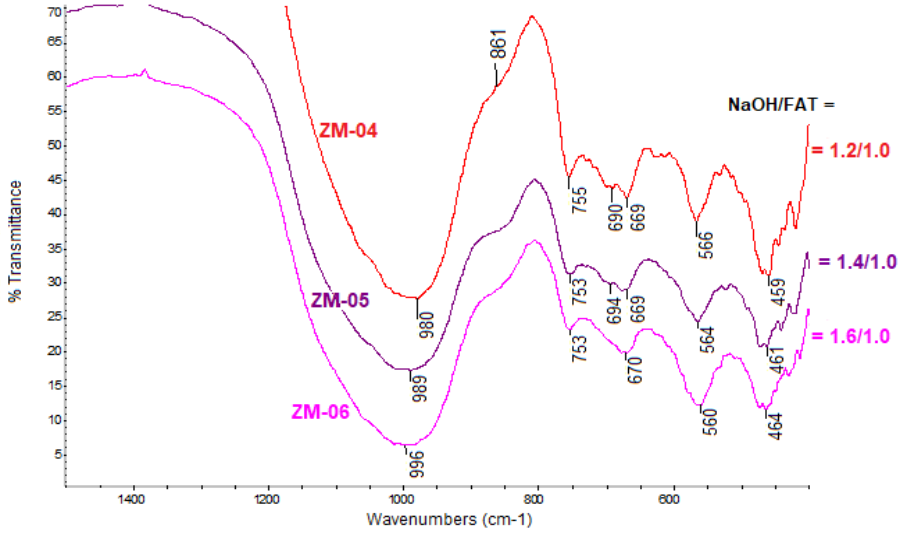

Figure 4. IR spectra of ZM-04, ZM-05 and ZM-06, obtained at 550 ºC and at three increasing NaOH/FAT ratios.

According to Table 3, as the NaOH/FAT ratio increases, the content of *zeolite A* also increases, from 13.1% (ZM-04) to 26.3% (ZM-06). Simultaneously, zeolite X decreases from 34.1 % to 22.9 %, respectively, in those samples. This behavior is reflected in the respective IR spectra of Figure 4, when the T-O bending band at 459 cm^{-1}, corresponding to zeolite X (ZM-04), was transformed into a bending band of 464 cm^{-1} typical of zeolite A, (ZM-06). Likewise, in sample ZM-04 the broad asymmetric stretching band of sodalite changed from 980 cm^{-1} to 996 cm^{-1}, which is the characteristic frequency of zeolite A, being concordant with the remarkable increase of this crystalline phase, as the NaOH/FAT ratio increased (Table 3). In addition, the weak shoulder band of symmetric stretching at 690 cm^{-1} in the spectra of zeolite X (ZM-04 and ZM-06) disappeared, indicating the decrease of this crystalline phase with the increase of the NaOH/FAT ratio. It was also observed that the medium band of symmetric stretching at 670 cm^{-1}, and the medium band at 560 cm^{-1} for the double ring D6R, both corresponding to zeolite X, are practically maintained in the three spectra of samples, despite the decrease of this phase and with the increase of the NaOH/FAT ratio. The symmetric stretching bands at 753 cm^{-1} and 670 cm^{-1} which appeared in the three spectra (Figure 4), correspond to the presence of *zeolite X* (Ojha, et al., 2004).

3.3.3 Zeolites MZ-07, MZ-08, MZ-09 and MZ-10

Figure 5 shows the IR spectra of sample ZM-07 (with FATH and melted at 550 ºC) and of samples ZM-08, ZM-09 and ZM-10 (obtained at 650 ºC, and with increasing ratios. of NaOH/FAT). These four samples are made up exclusively of zeolite A and zeolite *X* (Table 4), although as noted above, ZM-07 also has two different variants of production. Table 6 summarizes the values of the most relevant IR frequencies of the four zeolites samples, with the referential frequencies of Table 5. The data of Table 6 reveal that sample ZM-08 presents the structural characteristics of zeolites A and X, however, as the NaOH/FAT ratio increases, some of the zeolite X frequencies are attenuated: the flexion at 451 cm^{-1} and the stretching at 668 cm^{-1}.

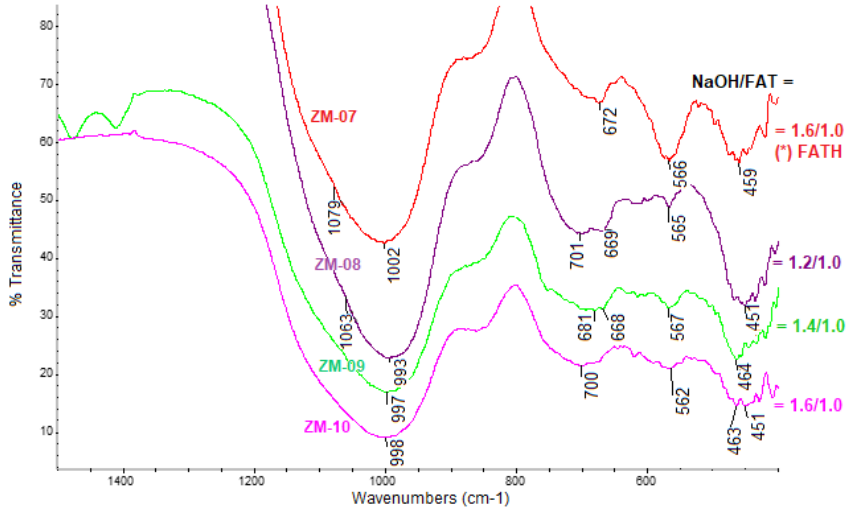

Figure 5. IR spectra of zeolitic sample ZM-07, ZM-08, ZM-09 and ZM-10.

Table 6. Peaks of IR spectral frequencies of Figure 5, which identify zeolite A and zeolite X

Sample (NaOH/CVT)	ZEOLITE - A				ZEOLITE - X			
	Stretching asymmetrical		Double ring	Bending T–0	Stretching asymmetrical	symmetrical	Double	Bending T–0
ZM-07 (1.6/1)*	1079 *vwsh*	1002*s*	--	--	- -	672*m*	566*m*	459*ms*
ZM-08 (1.2/1)	--	993*s*	--	--	1063*msh*	669*m*	565*m*	451*ms*
ZM-09 (1.4/1)	--	997*s*	--	464*m*	--	668*m*	567*m*	--
ZM-10 (1.6/1)	--	998*s*	--	463*m*	--	--	562*m*	451*ms*

* : zeolitic mixture from acid-fly ashes (FATH) and alkaline fusion at 550 ºC.

On the other hand, the strong band at 998 cm^{-1} and the bending at 464 cm^{-1} confirmed the presence of *zeolite A,* while the double ring band at 562 cm^{-1} indicated the presence of zeolite X, although the disappearance of zeolite band at 668 cm^{-1}. The increase in NaOH/FAT increases zeolite A and decreases *zeolite X*.

4. Conclusions

Fly ash with a high percentage of unburned may be used as a raw material to obtain a zeolitic material, which is mostly formed by *sodalite* phase, or by a mixture of *zeolite A* and *zeolite X*. At a lower melting temperature and at lower NaOH/CVT ratio, *sodalite* is formed as the majority phase. However, increasing the melting temperature, a mixture of *zeolite A* and *zeolite X* may be obtained. At higher temperatures, *zeolite A* increases with the rise of the NaOH/FAT ratio. A follow-up on the frequency changes of the IR spectra can confirm that the sodalite, zeolite A and zeolite X, come from the same polyhedral unit, and where the operating conditions that increase the amount of the last two, implies the decrease and disappearance of sodalite.

Acknowledgments

The authors gratefully thank the Peruvian Canon Minero support by the Project 098314042. The authors acknowledge the National Laboratory of Nano- and Biomaterials (LANNBIO-CINVESTAV), for allowing the use of SEM-EDS facilities; thanks also go to Biol. Ana R. Cristóbal R. and M.Sc. Dora A. Huerta Q., for their support in SEM-EDS data acquisition.

References

Akbelen M., 2021, Investigation of Natural Analcime-rich Zeolite Tuff from Turkey: A Combined XRD, XRF, FT-IR and SEM Study. Eskişehir Technical Univ. J. of Sci. and Tech. B – Theo. Sci., 9, 36-41.

Belviso C., Cavalcante F., Fiore S., 2010, Synthesis of zeolite from Italian coal fly ash: Differences in crystallization temperature using seawater instead of distilled water. Waste Management, 30, 839–847.

Byrappa K. and Yoshimura M., 2013, Handbook and Hydrothermal Technology; Second Edition, Elsevier Inc. United States of America. Chapter 6. Hydrothermal Synthesis and Growth of Zeolites. 269-347.

Byrappa K. and Yoshimura M., 2013, Handbook and Hydrotermal Technology; Second Edition, Elsevier Inc. United States of America. Chapter 6. Hydrothermal Synthesis and Growth of Zeolites. 269-347.

Chaves Lima R, Bieseki L, Vinaches Melguizo P., Castellã Pergher S.B, 2019, Environmentally Friendly. Zeolites. Synthesis and Source Materials. ©Springer Nature Switzerland AG 2019.

Duan A., Wan G., Zhang Y., Zhao Z., Jiang G., Liu J., 2011, Optimal synthesis of micro/mesoporous beta zeolite from kaolin clay and catalytic performance for hydrodesulfurization of diesel,Catalysis Today,175, 485– 493

Flanigen E.M. and Khatami H., SzymanskI Herman A. (1974) Infrared Structural Studies of Zeolite Frameworks. Molecular Sieve Zeolites-I. *Advances in Chemistry*; American Chemical Society. Pags: 201-229

Hartati, Prasetyoko D., Santoso M., Qoniah I., Leaw W.L., Firda P.B. D, Nur H (2020). A review on synthesis of kaolin-based zeolite and the effect of impurities. J. of The Chinese Chemical Society, 67, 6;1–26 (911-936).

Hermeler, G, Buhl J.CH., and Hoffmann W.,1991, The Influence of Carbonate on The Synthesis of an Intermediate Phase Between Sodalite and Cancrinite. Catalysis Today. 8, 415 – 426.

Janowska-Renkas E. and Kaliciak A.,2021, Impact of Fly Ashes from Combustion in Fluidized Bed Boilers and Siliceous Fly Ashes on Durability of Mortars Exposed to Seawater and Carbonation Process. *Materials,*14, 2345.

Loiola A.R, Andrade J.C.R.A, Sasaki J.M, Da Silva L.R.D, 2012, Structural analysis of zeolite NaA synthesized by a cost-effective hydrothermal method using kaolin and its use as water softener. Journal of Colloid and Interface Science, 36, 34–39

Ma S., Liu Z-P., 2022, The Role of Zeolite Framework in Zeolite Stability and Catalysis from Recent Atomic Simulation. Topics in Catalysis, 65, 59–68

Ojha Keka, Pradhan Narayan C and Samanta Amar Nath, 2004, Zeolite from fly ash: synthesis and characterization. Bulletin of Materials Science. 27, pp. 555–564.

Pengcheng Lv, Meng R., Mao Z. and Deng M., 2021, Hydrothermal Synthesis of Sodalite-Type N-A-S-H from Fly Ash to Remove Ammonium and Phosphorus from Water. *Materials*, 14, 2741.

Shi B. and Chang Q., 2021, Green synthesis of fly ash-based zeolite Y by mixed alkali fusion method. Micro Nano Lett, 16, 540–545.

Shigemoto N., Sugiyama S., Hayashi H. and Miyaura K., 1995, Characterization of Na-X, Na-A, and coal fly ash zeolites and their amorphous precursors by IR, MAS NMR and XPS. *J. of Mat. Sci.* 30, 5777 – 5783

Zhan, Bi-Zeng, White M.A., Lumsden M., Mueller-Neuhaus J., Robertson, K. N, Cameron T.S., and Gharghouri M., 2002, Control of Particle Size and Surface Properties of Crystals of NaX Zeolite. Chemistry of Materials, 14, 3636-3642.